Available online at www.sciencedirect.com
SCIENCE DIRECT®
International Journal of Thermal Sciences 42 (2003) 1089–1103
International Journal of Thermal Sciences
www.elsevier.com/locate/ijts

Heat transfer in a smooth-walled reciprocating anti-gravity open thermosyphon

S.W. Chang [a,*], L.M. Su [b], W.D. Morris [c], T.M. Liou [d]

[a] *Thermal Fluids Laboratory, National Kaohsiung Institute of Marine Technology, Kaohsiung, Post code: 811, Taiwan, ROC*
[b] *Department of Electrical Engineering, Tung Fang Institute of Technology, Taiwan, ROC*
[c] *Department of Mechanical Engineering, University of Wales Swansea, Singleton Park, Swansea SA28PP, UK*
[d] *Department of Power Mechanical Engineering, National Tsing Hua University, Hsinchu, Taiwan, ROC*

Received 18 July 2002; accepted 7 March 2003

Abstract

This paper describes an experimental investigation of heat transfer in a smooth-walled reciprocating anti-gravity open thermosyphon with relevance to the *'shaker'* cooling system for the pistons of marine propulsive diesel engines. A selection of experimental results illustrates the interactive effects of inertial, reciprocating and buoyancy forces on heat transfer. It is demonstrated that the gravitational and reciprocating buoyancy effects, respectively, improve heat transfer in the static and reciprocating anti-gravity open thermosyphon. The individual pulsating force effect impairs heat transfer in the axial region with 5 hydraulic diameter length measured from the entrance of thermosyphon (region I). In the vicinity of sealed end of reciprocating thermosyphon with one hydraulic diameter from the sealed surface (region II), the individual pulsating force effect improves heat transfer at low pulsating number range, over which range a subsequent heat transfer reduction in this axial region is followed. The synergistic effects of inertial force, reciprocating force and buoyancy interaction in the reciprocating anti-gravity open thermosyphon could, respectively, impede or improve the regional heat transfers in the axial regions I and II from the static references of zero-buoyancy. A set of empirical correlations, which is physically consistent, was developed that permits the individual and interactive effects of inertial, reciprocating and buoyancy forces on heat transfer to be evaluated.
© 2003 Éditions scientifiques et médicales Elsevier SAS. All rights reserved.

Keywords: Anti-gravity; Reciprocating; Thermosyphon; Piston cooling

1. Introduction

The propulsive system of a marine vessel widely adopts the heavy-duty Diesel engine, fueled by residual oil, which directly drives the propeller in order to obviate the use of heavy-duty reduction gearboxes. A higher propulsive efficiency of the propeller generally requires a lower speed. Therefore, a larger than normal stroke to bore ratio of marine propulsive Diesel engine is developed in order to achieve the low engine speed matching the characteristics of the engine to the directly driven propeller. As a representative example of this class of engine, the Sulzer RTA 60 C engine normally operates at a speed range of 91–114 rev·min^{-1} with maximum cycle pressure and temperature of about 155 bar and 1500 °C, respectively. An effective cooling scheme inside the piston is essential to ensure the structure integrity when considerably high thermal and mechanical loads are applied to the reciprocating piston. Fig. 1 typifies the multi-bore shaker cooling system in the pistons of the Sulzer RTA Diesel engine series. As shown, the coolant, fresh water, in each of these blind passages is convected "from" and "to" the plenum chamber in the tube-wise direction when the piston reciprocates. The plenum chamber acts as "reservoir" that provides a thermal sink for the coolant in the blind bores to exchange heat with the bulk flow in the plenum chamber. Note, the hot and cold sections of each blind bore locate, respectively, at its top and bottom ends. There is a tendency for the coolant to stratify, with regions of hot coolant *'trapped'* in the vicinity of the sealed end due to gravitational free convection when the system is static. This class of flow system has been referred to as *'anti-gravity open single*

* Corresponding author.
E-mail address: swchang@mail.nkimt.edu.tw (S.W. Chang).

1290-0729/$ – see front matter © 2003 Éditions scientifiques et médicales Elsevier SAS. All rights reserved.
doi:10.1016/S1290-0729(03)00090-5

Nomenclature

English symbols

a	reciprocating amplitude (crank radius)	m
A_s	entire heating surface	m^2
C_p	specific heat of coolant	$J{\cdot}kg^{-1}{\cdot}K^{-1}$
d	hydraulic diameter of test duct	m
Gr	Grashof number, $= g\beta(T_w - T_f)d^3/\upsilon^2$	
Gr_p	pulsating Grashof number, $= \omega^2 a\beta(T_w - T_f)d^3/\upsilon^2$	
H	Height of thermosyphon	m
H_p	height of plenum chamber	m
k_f	thermal conductivity of coolant	$W{\cdot}m^{-1}{\cdot}K^{-1}$
$\dot{m}$	coolant mass flow rate	$kg{\cdot}s^{-1}$
Nu	Nusselt number, $= (RePr\eta_w)(d^2/A_s)$	
p	flow pressure	$N{\cdot}m^{-2}$
p'	pressure perturbation due to reciprocating forces	
Pr	Prandtl number, $= \mu C_p/k_f$	
Pu	pulsating number, $= \omega d/W_m$ (pulsating-to-inertial force ratio)	
$\dot{Q}_f$	local convective heat	W
Re	Reynolds number, $= \rho W_m d/\mu$	
T	temperature	°C
T_0	fluid temperature at the open end of thermosyphon	°C
u, v, w	flow velocities	$m{\cdot}s^{-1}$
U, V, W	dimensionless flow velocity vector, $= v/W_m$	
W_d	width of plenum chamber	m
W_m	mean flow velocity, $= \dot{m}/\rho d^2$	$m{\cdot}s^{-1}$
z	axial coordinate	m
Z	dimensionless axial location, $= z/d$	

Greek symbols

$\varphi, \Phi, \Psi_1, \Psi_2$	unknown function	
β	thermal expansion coefficient of coolant	K^{-1}
ρ	density of coolant	$kg{\cdot}m^{-3}$
η	non-dimensional temperature	
υ	kinematic viscosity of coolant	$m^2{\cdot}s^{-1}$
τ	dimensionless time, $= \omega t$	
ω	angular velocity of rotating disc creating reciprocating motion	$rad{\cdot}s^{-1}$
χ	dimensionless flow pressure	

Subscripts

f	fluids
w	wall
ZB	zero-buoyancy condition

Superscript

0	static condition

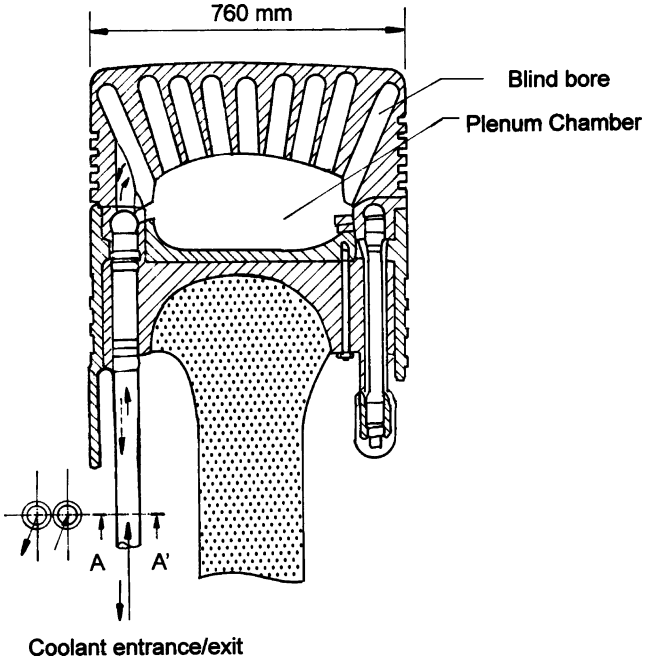

Fig. 1. Shaker cooling network in Sulzer RTAT6 marine propulsive diesel engine.

phase thermosyphon' in the technical literature [1]. The additional superimposed effect of reciprocation on the system has led to the 'shaker' piston cooling method to be categorized as a *'reciprocating anti-gravity open thermosyphon'*. When the tube-wise directions of the inclined blind-bores are no longer parallel to the reciprocating forces, temporally varying cross-plane secondary flows are also induced which are not dealt with in this work.

Studies of static open cavity flows have demonstrated that the penetration of coolant circulation in each blind passage is influenced by the flow pattern across its open surface and also by the geometrical features of the passage and the plenum chamber [2,3]. Increasing the length-to-width ratio of the cavity (i.e., a deeper cavity) generally increases the vortices formed in the passage and weakens the vortex in the vicinity of the sealed end [4]. During the transient development of the flow over the open cavity, the rate of mass exchange of the fluid inside the cavity is enhanced [4]. When the periodicity of the buoyancy forces in the closed cavity flow is introduced (either by the periodical heating condition [5,6] or by the vibration of solid boundary [7–10]) rich vortical flow structures are established in these enclosures. The processes of vortex generation, convection and diffusion for these cavity flows are dynamic and depend on the oscillating frequency and amplitude of the boundary conditions imposed [7–11]. The various modes of temporal variations in flow pattern caused by varying the vibration frequency generate several different thermal convection regimes in a vibrating enclosure [9,10]. The increase of vibration frequency generally improves heat transfer in a vibrating enclosure.

But, in the so-called flow regime of intermediate convection regime, the increase of vibration frequency could reduce heat transfer [9]. Although the studies of vibrational cavity flows [4–11] share a degree of similarity with the shaker cooling geometry depicted in Fig. 1, subtle differences exist between the reciprocating forces, and the flow interactions initiated in the open-end region of each blind bore of the piston shaker-cooling networks. Thus, the lack of fundamental knowledge concerning the performance of this particular cooling geometry, despite its apparent engineering application, has been the motivation for the present investigation.

This experimental study examines the effect of reciprocation on heat transfer in a vertical square sectioned smooth-walled anti-gravity open thermosyphon with geometries simulating a blind passage of shaker cooling network shown in Fig. 1. The direction of the reciprocation is along the central axis of the open thermosyphon tube. The governing dimensionless flow parameters of the reciprocating anti-gravity open thermosyphon are identified through the parametric study as the first step following which the procedures of data reduction and experimental program are determined and the experimental apparatus is built. The detailed flow distributions inside a reciprocating open thermosyphon are influenced by the reciprocation, the flow pattern across its open surface and also by the geometrical features of the passage and the plenum chamber. The controlled geometries therefore involve the thermosyphon and plenum chamber. At each cross-sectioned plane of the thermosyphon tube, the mass conservation requires a zero mean flow velocity. This has led a difficulty to define the local Reynolds number using the mean flow velocity inside the thermosyphon. Also the mean flow temperature over the cross plane of thermosyphon is a dependent variable of the governing non-dimensional flow and geometrical parameters. Nevertheless, by treating the values of local flow velocity and mean flow temperature over a cross-sectioned plane of thermosyphon as the dependent variables, the control of fluxes of heat and coolant mass flow fed into the system and the reciprocating frequency for a given set of geometrical and heating conditions could specify a particular flow and heat transfer patterns. The characteristic flow velocity is conveniently evaluated in accordance with the total mass flux fed into the plenum chamber and the characteristic length selected. For any given total mass flow rate through the present test geometry, the temperature rise of fluid from the entry to the exit plane of the present thermo fluids system varies with the heating rate. The temperature difference between the flow entrance and exit of the test geometry is selected as the characteristic temperature scale to normalize the temperature measurements. In what follows, the governing dimensionless groups identified from a set of generalized dimensionless flow equations, the data reduction procedure and the concept of dimensionless temperature, which is particularly convenient for engineering application, are illustrated in details.

2. Generalized dimensionless flow equations and method of data reduction

Fig. 2 illustrates the simplified geometric flow system being studied to simulate the ‘shaker’ piston-cooling concept. The thermosyphon tube and the fluid reservoir oscillate together and coolant flows into and out of the reservoir as illustrated in the figure. The thermosyphon tube is square in cross section with smooth walls as shown. The two sidewalls are uniformly heated and the other two opposite walls are adiabatic. The non-dimensional groups that describe the physical processes present in this flow/heat transfer system may be derived as follows.

The oscillatory motion produced by the engine piston is not truly sinusoidal and depends on the ratio of the connecting rod length to the crankshaft. However when this ratio is greater than eight, the reciprocating motion is well approximated as ‘simple harmonic’ in nature. In this case the oscillatory motion of the flow system may be described as

$$z = a \cdot \sin(\omega t) \tag{1}$$

Consider the Cartesian coordinate reference frame shown in Fig. 2. The origin of the frame oscillates and the fluid velocity components relative to this origin are u, v and w in the coordinate directions x, y and z, respectively. The z-direction momentum conservation equation for a fluid having constant properties may be written as

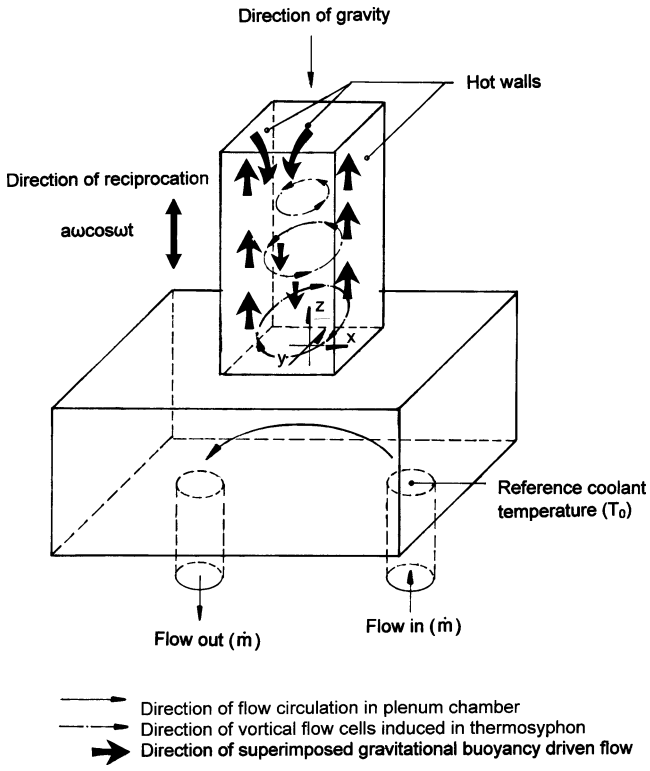

Fig. 2. Conceptual flow geometry and boundary conditions simulated for a reciprocating anti-gravity open thermosyphon.

$$\rho_0\left(\frac{\partial w}{\partial t}+u\frac{\partial w}{\partial x}+v\frac{\partial w}{\partial y}+w\frac{\partial w}{\partial z}\right)$$
$$=-\nabla p+\mu_0\nabla^2 w-\rho_0\big(g+a\omega^2\sin(\omega t)\big) \quad (2)$$

The fluid density and viscosity are evaluated at a reference temperature, T_0.

For this case of constant property flow, the effect of the reciprocation may be considered as an effective body force (i.e., an artificial time dependent gravity). Thus, for the case of zero flow, the pressure generated inside the system will be a modified gravitationally induced hydrostatic pressure, p_0, given by

$$\frac{\partial p_0}{\partial z}=-\rho_0\big(g+a\omega^2\sin(\omega t)\big) \quad (3)$$

If the fluid has a temperature sensitive density, heating of the fluid will create buoyancy forces via gravity and the reciprocating effective body force. The density, ρ, of the fluid, at any temperature T, may be linked to the reference density via an equation of having the form

$$\rho=\rho_0\big(1-\beta_0(T-T_0)\big) \quad (4)$$

where β_0 is the coefficient of cubical expansion of fluid evaluated at the reference temperature, T_0.

Insertion of Eq. (4) into Eq. (2) and introducing the Boussinesq approximation yields

$$\left(\frac{\partial w}{\partial t}+u\frac{\partial w}{\partial x}+v\frac{\partial w}{\partial y}+w\frac{\partial w}{\partial z}\right) \quad (5)$$
$$=-\frac{1}{\rho_0}\nabla p'+\nu_0\nabla^2 v-\beta_0(T-T_0)\big(g+a\omega^2\sin(\omega t)\big)$$

where p' is the algebraic difference between the true pressure and the hydrostatic pressure specified by Eq. (2). Note that, the last term in Eq. (5) involves two acceleration fields, namely the gravitational and reciprocating accelerations, which feature two physically different buoyancy interactions. The influence of gravitational buoyancy normally develops in the steady flow field among which the differences in fluid temperature are stable and the differences in volumetric gravity force over the cross-sectioned plane of thermosyphon promote fluid motion in static condition. The buoyancy term $\beta_0(T-T_0)a\omega^2\sin(\omega t)$, motivated by the reciprocating acceleration, features the complex buoyancy interactions in a quasi-steady flow. The implementation of curl operation through Eq. (5) converts the momentum equation into an equation describing the vorticity transportation. The term $\nabla\times(\beta_0(T-T_0)a\omega^2\sin(\omega t))$ remains as a source term to generate vorticity, which is a sign-varied temporal function. It is felt that the buoyancy interactions in the present reciprocating case are originated from their effects on the vorticity. The temporary varied vorticity field affected by the reciprocating buoyancy could lead to a different mode of buoyancy interaction from the gravitation associated buoyancy effects. Thus the gravitational buoyancy is unlikely to exert considerable effect on flow and heat transfer inside a reciprocating thermosyphon as the flow and temperature fields are never steady. Therefore the gravitational and reciprocating accelerations are separately summarized in the last two terms on the right-hand side of Eq. (5) that, respectively, dominates the buoyancy interactions in static and reciprocating thermosyphon. It is very unlikely to develop the free convective type flow that is typical in steady flow system and the reciprocating buoyancy simultaneously.

The conservation of energy equation is

$$\frac{\partial T}{\partial t}+u\frac{\partial T}{\partial x}+v\frac{\partial T}{\partial y}+w\frac{\partial T}{\partial z}=\frac{k_0}{\rho_0 C_{p,0}}\nabla^2 T \quad (6)$$

The non-dimensional groups that parametrically govern the flow and temperature fields may be determined using the following transformations of the dependent and independent variables.

$$X=\frac{x}{d},\qquad Y=\frac{y}{d},\qquad Z=\frac{z}{d} \quad (7)$$

$$U=\frac{u}{W_m},\qquad V=\frac{v}{W_m},\qquad W=\frac{w}{W_m} \quad (8)$$

$$\chi=\frac{p'}{\rho_0 W_m^2},\qquad \eta=\frac{T-T_0}{\Delta T_f},\qquad \tau=\omega t \quad (9)$$

In Eqs. (8) and (9) d is a characteristic system length, conveniently taken to the hydraulic diameter of the square sectioned thermosyphon tube, W_m is a characteristic fluid velocity defined as

$$W_m=\frac{\dot m}{\rho_0 d^2} \quad (10)$$

where $\dot m$ is the total coolant flow rate passing through the reservoir, and ΔT_f is the temperature rise of the fluid passing through the reservoir given by

$$\Delta T_f=\frac{\dot Q_f}{\dot m C_{p,0}} \quad (11)$$

where $\dot Q_f$ is the heat transfer rate through the surface of the thermosyphon tube.

If the transformations given in Eqs. (7)–(9) are inserted into Eqs. (5) and (6) we get, after some routine algebraic manipulation, the following parametric form of the axial momentum conservation equation and the energy equation.

$$Pu\frac{\partial W}{\partial \tau}+\left(U\frac{\partial W}{\partial X}+V\frac{\partial W}{\partial Y}+W\frac{\partial W}{\partial Z}\right)$$
$$=-\frac{\partial \chi}{\partial Z}+\frac{1}{Re}\nabla^2 W+\frac{1}{Re_g^2}\big(Gr_g+Gr_p\sin(\tau)\big) \quad (12)$$

$$Pu\frac{\partial \eta}{\partial \tau}+U\frac{\partial \eta}{\partial X}+V\frac{\partial \eta}{\partial Y}+W\frac{\partial \eta}{\partial Z}=\frac{1}{Re\,Pr}\nabla^2\eta \quad (13)$$

where

$$Re=\frac{W_m d}{\nu_0}\quad \text{(Reynolds number)} \quad (14)$$

$$Pu=\frac{\omega d}{W_m}\quad \text{(pulsating number)} \quad (15)$$

$$Gr_g=\frac{g\beta_0 d^3\Delta T_f}{\nu_0^2}\quad \text{(gravitational Grashof number)} \quad (16)$$

$$Gr_p = \frac{a\omega^2\beta_0 d^3 \Delta T_f}{\nu_0^2} \quad \text{(pulsating Grashof number)} \tag{17}$$

$$Pr = \frac{\mu_0 C_{p,0}}{k_{f,0}} \quad \text{(fluid Prandtl number)} \tag{18}$$

The non-dimensional parameters given by Eqs. (14)–(18) govern the heat transfer and flow in this system. The Reynolds number, *Re*, may be interpreted as the ratio of fluid inertial forces to viscous forces in the usual manner. The Pulsating number, *Pu*, has its origin in the transient term of the total derivative of the momentum equation and expresses the ratio of the transient inertial forces, induced by the reciprocation, to the fluid inertial force. The gravitational Grashof number, Gr_g, expresses the ratio of the buoyancy forces due to the earth's gravitational field to viscous forces. The pulsating Grashof number, Gr_p, which features the buoyancy interactions in a unsteady flow field, expresses the ratio of the buoyancy forces due to the effective body force field created by the reciprocation to viscous forces. The Prandtl number, *Pr*, characterizes the fluid in the usual manner.

Because the fluid velocities, U, V, and W are interrelated in the convective term of momentum equation, the variation in axial velocity, W, due to reciprocation also affects the velocities of U and V. The above argument suggests that the non-dimensional fluid velocities, U, V, and W, and the non-dimensional temperature at the interface of fluid and heated wall, η_w, may be expressed as

$$U, V, W = U, V, W(X, Y, Z, Re, Pu, Gr_g, Gr_p, Pr) \tag{19}$$

$$\eta_w = \eta_w(X, Y, Z, Re, Pu, Gr_g, Gr_p, Pr) \tag{20}$$

The solutions of Eqs. (19) and (20) are also subject to the hydrodynamic, thermal and geometric boundary conditions at the interface between the solid–wall and the coolant flow. These boundary conditions include the specific internal geometries of the duct selected (i.e., the cross-sectional shape and length of the thermosyphon tube together with a full geometric description of the wall surface and also the plenum chamber geometry). It is worth noting that, in actual marine RTA engine, the water is used as the coolant, which could yield the heat transfer results due to the additional convective boiling phenomena and the heat transfer impacts of variations in Prandtl number. This study is formulated as a preliminary study to explore the impacts of *Re*, $Gr_{g,p}$ and *Pu* on heat transfer with the Prandtl number effects and boiling phenomena isolated from the present investigation. It is attempted to unravel the heat transfer impacts of *Re*, $Gr_{g,p}$ and *Pu* in Eq. (20) that provides the basic understanding before the influences of convective boiling phenomena, accompanying with the variable *Pr* effects on heat transfer in a reciprocating anti-gravity open thermosyphon to be explored. Therefore the air was selected as the test coolant that rules out the convective boiling phenomena. As the variation of Prandtl number for air is small over the range of temperature covered by the experimental program undertaken, the influence of Prandtl number may be conveniently removed from Eqs. (18) and (19).

Based on the physical argument described above the experimental program is designed to permit the z-wise temperature distribution along one heated walls of the thermosyphon tube to be examined over a range of flow and reciprocation conditions. These measurements are made on the centerline of the heated wall. Thus, for a given geometrical configuration, the measured non-dimensional wall temperature, $\eta_w(Z)$, is expected to be functionally related to the Reynolds number, the pulsating number, the gravitational Grashof number and the pulsating Grashof number in some manner.

The interpolation and correlation of heat transfer results in terms of non-dimensional wall temperature, η_w, offer a direct measure of temperature solution at the interface of coolant and heated wall. When the reference fluid temperature, T_0, is customarily selected as the flow temperature at the entrance of a thermal fluid system, the conventional Nusselt number is related with non-dimensional wall temperature, η_w, as

$$\eta_w(Z) = \frac{RePr}{Nu(Z)} \frac{d^2}{A_s} = \varphi[Z, Re, Pu, Gr_g, Gr_p] \tag{21}$$

where A_s is the entire heated surface area of the thermosyphon tube and φ is some functional relationship between the relevant non-dimensional numbers. The ratio of d^2/A_s for the tested open thermosyphon is 0.0769. It is worth noting that the reference fluid temperature selected for evaluation of Nusselt number in this case is T_0, which offers convenience for engineering applications.

The experimental raw data are processed into the dimensionless groups of Eq. (21). The convective heating power, $\dot{Q}_f$, used for calculating the temperature difference, ΔT_f, is obtained by subtracting the external heat loss from the total heating power. The heat loss is evaluated based on the results from a series of heat loss calibration runs. For tests at the highest temperature setting and reciprocating frequency, the estimated heat loss during an experiment was about 16.7% of the total heating power supply. The local coolant thermal and transport properties (i.e., density, constant pressure specific heat, thermal conductivity and viscosity) are evaluated by means of standard polynomial curve fitting functions using the measured fluid temperature at the flow entrance of plenum chamber. The isolated influence of each controlling parameter in Eq. (21) on the dimensionless wall temperature, η_w, is examined by varying one controlling variable with the other parameters remaining constants. The strategic aim of the present study is to identify φ function through two data generation phases and a detailed data analysis phase.

3. Experimental details

3.1. Apparatus

A brief description of the reciprocating facility and a detailed description of test geometry are now presented. Fig. 3 shows a schematic drawing of the reciprocating facility, which has been previously reported [12]. As shown, cooling air fed from a compressor unit (1) was directed into heat-transfer test module (2) through two control valves (3, 4), a float-type volume flow meter (5), a digital pressure gauge (6), and a flow calming tube (7). A thermocouple, which penetrated into the pipeline after the flow meter (5), measured the flow temperature for the evaluation of coolant mass flow rate. Adjustment of the needle valve (4) determined the flow rate required to achieve the pre-defined Reynolds number, *Re*, value. The coolant was vented through the exit pipe of the heated test module after it passed through the heated test section. The reciprocating motion of the test module (2) was created by a crank-wheel mechanism driven by a 1 500W DC electrical motor (8). Using the pulley-belt unit (9) and the gear box (10), the flywheel (11) could be controlled to a desired rotational speed. A counter balance weight (12) was fixed on the rotating wheel (10) in order to maintain dynamic balance during the reciprocating tests. An optical encoder (13) was installed on the shaft to measure the rotational speed for the evaluations of Pu and Gr_p.

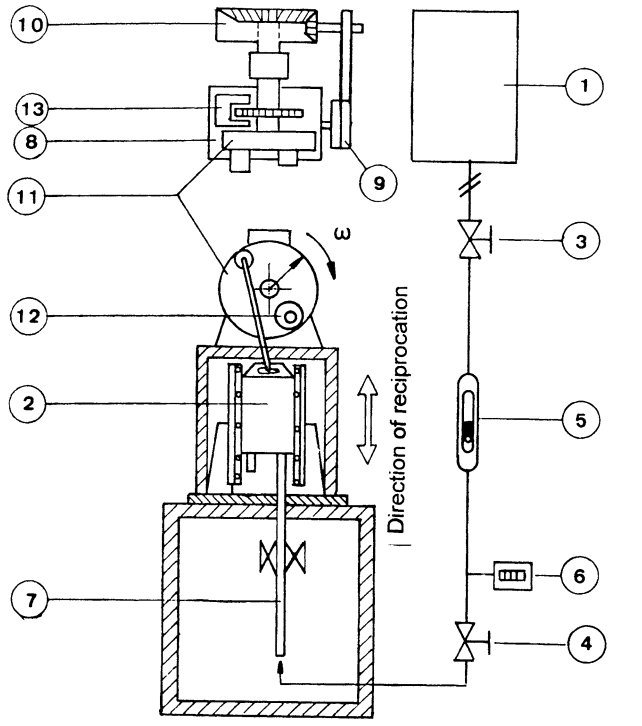

(1) Compressor unit (2) Heat transfer test module
(3) Stop valve (4) Needle valve
(5) Flow meter (6) Pressure gauge
(7) Flow calming tube (8) Electrical motor
(9) Pulley-belt unit (10) Gear box
(11) Fly wheel (12) Balance weight
(13) Optical pick-up

Fig. 3. Schematic diagram of reciprocating test facility.

Fig. 4 shows the constructional details of the square sectioned anti-gravity open thermosyphon actually tested. Two opposite smooth heated walls, and the sealed-end heating-surface, were made of a continuous 15 mm wide, 0.1 mm thick stainless steel foil (1). This heating foil (1) was clamped between four Tufnol sidewalls (2) to secure its position in the thermosyphon. The two ends of the heating surfaces were fixed on to the Tufnol bottom wall of thermosyphon (3) at which an electrical supply was connected to directly heat the smooth-walled stainless steel foils. A high-current, low-voltage DC electrical power supply was directly fed through the heating foil (1) to generate the uniform flux heating condition. Starting from the center of the top sealed surface (4), twelve K-type thermocouples were welded on the back of the stainless steel heating foil (1) to measure the wall temperatures. The 100 mm wide Tufnol bottom wall (3) with four height of 50 mm Tufnol sidewalls (5) formed a square-sectioned plenum chamber (6). A circular-sectioned coolant entrance tube (7) and an exit tube (8) permitted cooling air to be fed through the reservoir. These tubes were 12 mm in diameter and wee flush fitted to the bottom end of plenum chamber (9). The centers of the flow entrance and exit tubes (7, 8) were located 32.5 mm from the inner sidewalls of plenum chamber (5). Two thermocouples, respectively, penetrate into the centers of the flow entrance and exit tubes (7, 8), which measure the flow temperatures into and out of the test module. The temperature rise of the fluid passing through the reservoir, ΔT_f, was given by the temperature difference between the measurements of these two thermocouples. A routine check for ΔT_f was constantly performed using Eq. (11) in order to ensure the energy balance. The maximum discrepancy between the measured and calculated values of ΔT_f was selected as $\pm 10\%$ over which the data batch generated was abandoned. Four draw bolts (10) tightened the complete test assembly, which was encapsulated within a stiffening tube (11). An in fill of thermal insulation material packed in the space between the test section and the stiffening tube (11) minimizes external heat loss. The built up heat transfer test module was vertically mounted onto the reciprocating facility so that the anti-gravity open thermosyphon situation was simulated. The length and hydraulic diameter of the test section are 90 mm and 15 mm, respectively. Geometric features of the heat transfer test section have been specified in Table 1.

Note it is clear that the detailed geometries of sealed thermosyphon, plenum chamber and the entry/exit piping configurations could considerably affect the local heat transfers in thermosyphon. The primary task of present study is to unravel the thermal fluid physics of anti-gravity reciprocating thermosyphon with a specific set of thermal and geometri-

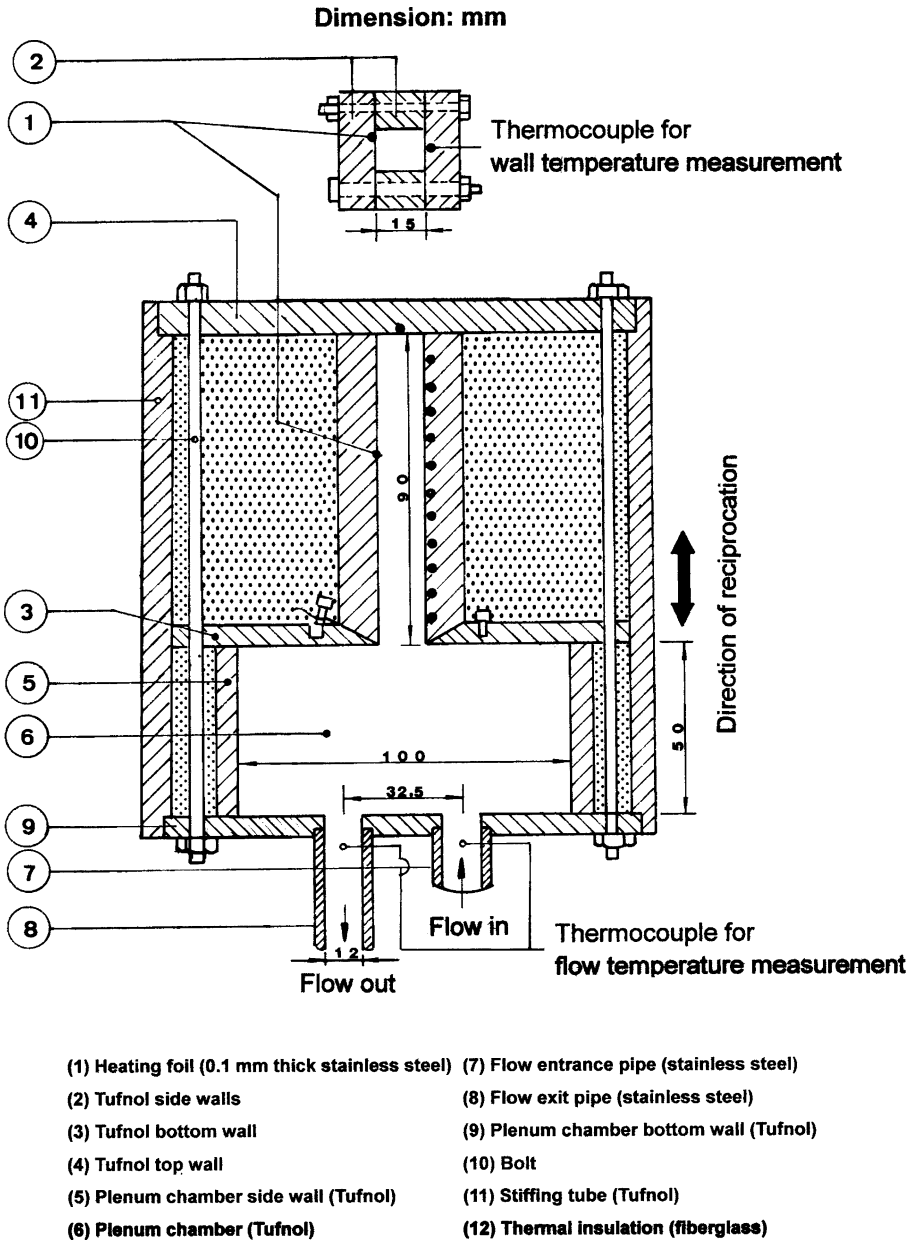

Fig. 4. Constructional details of heat transfer test module.

Table 1
Geometric features of test section

Geometric feature	Dimension (mm)
Height of thermosyphon (H)	90
Hydraulic diameter of thermosyphon (d)	15
Height of plenum chamber (H_p)	50
Width of plenum chamber (W_d)	100
Geometrical dimensionless groups	**Dimensionless ratio**
Aspect ratio of thermosyphon (d/H)	0.167
Aspect ratio of plenum chamber (W_d/H_p)	2

cal boundary conditions define by the test section depicted in Fig. 4. The methodology developed in this study to analyze the heat transfer data, which could lead to the generation of empirical heat transfer correlation formulate the primary goal of present study. When the geometrical features of thermosyphon unit vary for different design applications, the coefficients in the empirical correlations will be accordingly modified. The devised methodology could also be applicable when the detailed test geometries specified in Fig. 4 are adjusted.

An electrical power control of heating power provided the required heating current. Adjusting the heating power supply varies the relative strength of the overall buoyancy level at any fixed flow condition. All the temperature measurements were monitored and stored in a DX33 PC using a Net-Daq Fluke Hydra 2640A-100 data logger for the subsequent data processing. This data logging system provides 300 scans in

one second. The resolution and accuracy of thermocouples are respectively 0.01 °C and +0.1 °C.

3.2. Experimental program

This experimental program has three phases:

(1) Initially the heat transfer performance of the static anti-gravity open thermosyphon was investigated. In this way, the gravity-driven buoyancy effect on heat transfer is particularly studied. The extrapolated results with zero buoyancy based on the data generated in this phase are treated as the asymptotic solutions of zero reciprocation and zero buoyancy for the data analysis in the third phase.
(2) The second phase involved a systematic investigation of the combined effect of the reciprocating buoyancy together with the system reciprocation. The range of experimental parameters covered was typical of those encountered in the real engine case.
(3) The third phase involved an attempt to generate empirical correlations to permit all the relevant physical effects governing the system's behavior to be examined. Thus, the interactive effect of the buoyancy and the effective body force created by the reciprocation together with a transient inertial force due to reciprocation has been unraveled.

Note, because the viscosity and density of the coolant varied with the temperature, the mass flow rate was adjusted to limit variations of the Reynolds and pulsating numbers (at the entrance of the plenum chamber), to within ±1% of the nominal values selected.

Initially the instrumentation and data reduction program were checked out, with a series of static baseline heat transfer experiments. Correlations of the local heat transfer, in terms of the Reynolds number and gravitational Grashof number, were determined for this static benchmark phase. This phase was followed by a series of reciprocating experiments. The reciprocating data was produced at a fixed value of Reynolds numbers. At each selected Reynolds number, five sets of tests at the reciprocating frequencies of 0.83, 1.25, 1.67, 1.83 and 2 Hz were performed. The data generated in this manner revealed the effect of reciprocation on heat transfer. At each selected Reynolds/pulsating number combination, five different levels of heating power, (which raised the wall temperature, at the sealed end of thermosyphon tube, to nominal levels of 50, 75, 100, 110 and 120 (130) °C, respectively), were used to systematically vary the effect of buoyancy by creating a range of gravitational and pulsating Grashof numbers.

The on-line data acquisition system collected and stored the instantaneous temperature measurements for every period of 10 seconds. These measurements were subsequently time-averaged and the averaged data were printed on the screen of PC for scanning. A quasi-steady state condition was assumed when the variations of the time-averaged wall temperatures remained with in ±0.3 °C. A period of about 45 minutes was required to achieve a quasi-steady state condition.

Table 2
Range of experimental non-dimensional parameters

Non-dimensional parameter	Range
Reynolds number	3500–9200
Pulsating number	0–0.04
Gravitational Grashof number	530–2700
Pulsating Grashof number	420–4500

The range of non-dimensional parameters covered is given in Table 2.

An analysis of the experimental uncertainties for this apparatus and method of data reduction has been undertaken [13]. As the equilibrium state of reciprocating thermosyphon flow system was approximated when the local wall temperature variations were in the range of ±0.3 °C, the maximum uncertainty in temperature measurement was estimated to be ±0.3 °C. The maximum percentages of error for the coolant's specific heat, mass flow rate and thermal conductivity and the fluid density were estimated as ±0.03%, ±3.8%, ±0.21%, and ±0.31% respectively. With the temperature difference between wall and fluid reference condition varied from 35 to 88 °C, the maximum uncertainty in η_w, Re, Pu, Gr_g and Gr_p were 12.7%, 6.7%, 2.3%, 5.1% and 6.8%, respectively.

4. Results and discussion

4.1. Static thermosyphon

In the absence of reciprocation, Eq. (21) shows that the local heat transfer in the static anti-gravity open thermosyphon is dependent on Re and Gr_g. Fig. 5 shows the Z-wise distributions of dimensionless wall temperature obtained with three different values of Gr_g at the fixed Reynolds numbers of 5300, 7100 or 9200. Referring to Figs. 5(a)–(c), we note that the region of highest dimensionless wall temperature occurs in the sealed end of the thermosyphon tube. The anti-gravity nature of this stationary thermosyphon appears to suppress convective movement of the fluid with a tendency for the coolant to stratify within this region of high temperature. In this region of high temperature ($Z > 5$), a pair of tube-wise vortical flow cells that is typical in a closed long-cavity [1] facilitates heat transfer. Note, the measurement made at $Z = 6$ is at the central point of the top-end sealed surface. Due to the penetration of coolant into the thermosyphon tube from the plenum chamber via coherent vortical flow cells induced by the cross-flow over the entrance of thermosyphon [4], the lower dimensionless wall temperatures in the entrance region are consistently observed. As shown in Fig. 5, the downward data spreads driven by increasing Gr_g demonstrates the improved heat

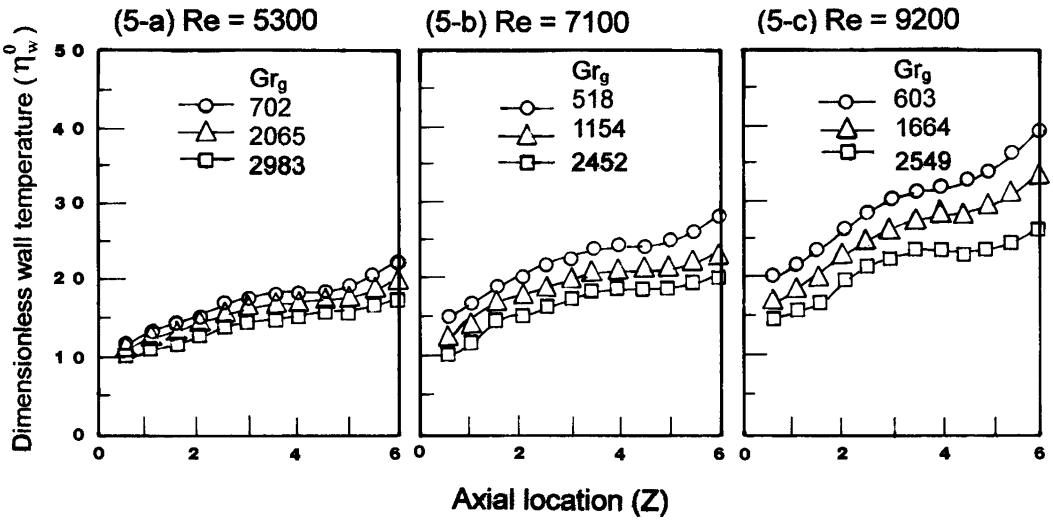

Fig. 5. Typical axial distributions of dimensionless wall temperature in static thermosyphon.

transfer due to buoyancy interaction. Note, the difference in the non-dimensional wall temperatures driven by the variation of Gr_g at a given axial location tends to reduce when Z value or Reynolds number decreases. This suggests that the effect of buoyancy is becoming less important in the entry region of the thermosyphon. The induced circulation of fluid that effectively transports the heat transferred from the tube surface to the plenum chamber dominates entry-region heat transfer so that the development of low dimensionless wall temperatures in the region of $Z < 2$ is accompanied with less small data spreads driven by buoyancy variation. At the higher Reynolds number value of 9200 shown in Fig. 5(c), this feature is still pronounced.

The main observations that may be made from the results shown in Fig. 5 are that the movement of fluid through the reservoir induces the coherent vortical flow cells in the entry region of the thermosyphon tube and that this circulation enhances with increases in the Reynolds number. Thus, the local wall to fluid heat transfer will be very much influenced by this induced flow circulation in the vicinity of the tube entrance. Additionally there is a clear superimposed effect of buoyancy, as characterized by the gravitational Grashof number. Local heat transfer is significantly increased by buoyancy particularly in the vicinity of the sealed end of the thermosyphon tube. Two interacting flow mechanisms control the heat transfer characteristics of this form of closed anti-gravity thermosyphon. Firstly, vortical flow cells induced in the entry region of the thermosyphon tube occur due to the continuous circulation of fluid through the reservoir. Secondly, the temperature- dependent fluid density combines with the gravitational force to produce a free convection effect. An attempt has been made to determine a correlating equation, in terms of the relevant non-dimensional parameters discussed in Section 2.2. The structure of this correlating equation has to be mathematically consistent with the controlling physics. In the limiting case

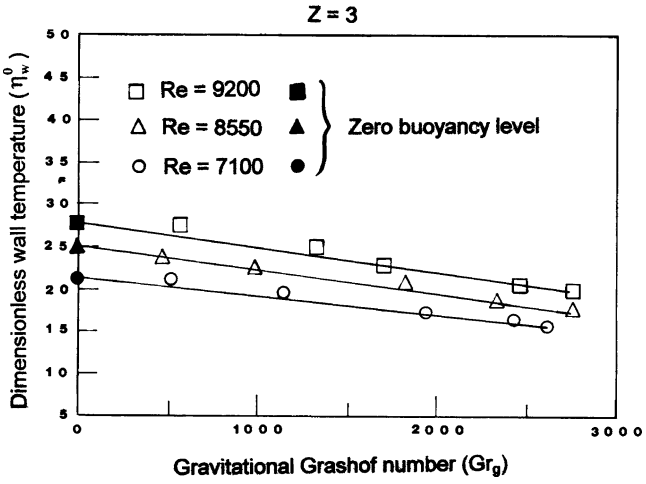

Fig. 6. Variation of dimensionless wall temperature with gravitational Grashof number in static thermosyphon with Reynolds numbers of 7100, 8550 and 9200 at axial location $Z = 3$.

of zero buoyancy, the heat transfer mechanism is entirely controlled by the induced flows from the reservoir so that

$$\eta^0_{wZB} = \Phi(Z, Re) \tag{22}$$

where η^0_{wZB} is the zero buoyancy asymptotic dimensionless wall temperature in the static thermosyphon and Φ is an, as yet, undetermined function of the axial location and Reynolds number.

Fig. 6 shows an illustrative example to demonstrate the procedure of revealing zero buoyancy asymptotic dimensionless wall temperature data. At each measuring station, the local dimensionless wall temperature decreases with increasing gravitational Grashof number for a given Reynolds number. These individual curves were numerically extrapolated back to the origin to determine the zero buoyancy dimensionless wall temperature for each axial location where measurements were made. The variation of the zero buoyancy dimensionless wall temperature with Reynolds number

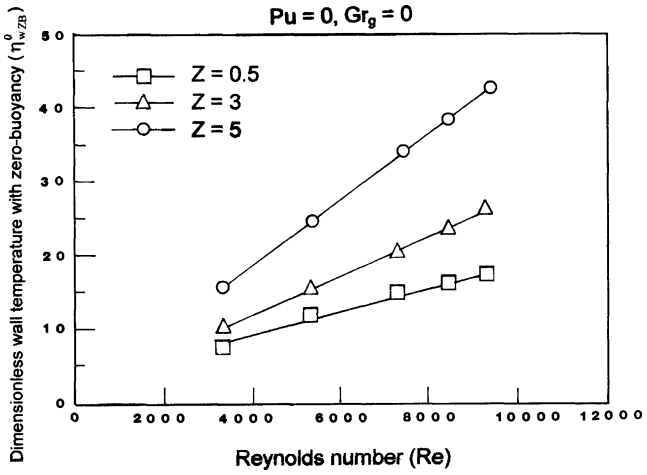

Fig. 7. Variation of dimensionless wall temperature at zero-buoyancy level with Reynolds number for axial locations 0.5 and 5Z.

Table 3
Correlations of η^0_{wZB} in static thermosyphon

Z	$\eta^0_{wZB} = A(Z) \times Re^{B(Z)}$	
	$A(Z)$	$B(Z)$
0.5	3.437E−2	0.6808
1	1.249E−2	0.8081
1.5	5.082E−3	0.9181
2	2.933E−3	0.98
2.5	2.955E−3	0.98
3	3.104E−3	0.99
3.5	3.314E−3	0.992
4	3.132E−3	0.999
4.5	3.087E−3	1.002
5	3.001E−3	1.011
5.5	4.703E−3	0.998
6	6.093E−3	0.996

at three measurement locations is also shown in Fig. 7. These individual curves were correlated using a power form and the results for each axial location is given in Table 3.

Referring to Eq. (21), when the Reynolds number is zero, the extrapolated zero-buoyancy asymptotic dimensionless wall temperature value corresponds to zero value of Nusselt number. Also the dependency of Nusselt number on Reynolds number vanishes when the power index $B(Z)$ become unity. Heat transfer in the limiting case of zero buoyancy with $B(Z) = 1$ features vanished *Re* effect. In this case, wall to fluid heat transfer is completely facilitated by thermal conduction and diffusion. Justified by the numerical results of $B(Z)$ shown in Table 3, the vanished *Re* effect prevails in the axial region of $Z > 2.5$. Following the argument in Section 2.1, the dimensionless parameters, Gr_g and Gr_p characterize two different modes of buoyancy interactions, which could not exist simultaneously. Thus Eq. (22) is treated as the zero buoyancy asymptotic heat transfer solution in reciprocating thermosyphon with $Pu = 0$.

Fig. 8 shows the combined *Re* and Gr_g effects on dimensionless wall temperatures at axial location of $Z = 3$. All the dimensionless wall temperature data could be well

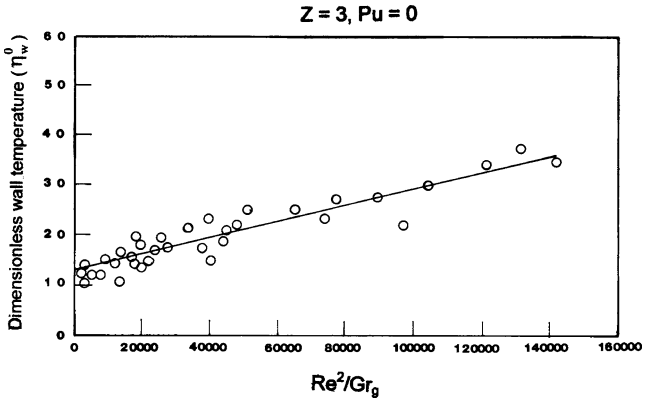

Fig. 8. Variation of dimensionless wall temperature with Re^2/Gr_g in static thermosyphon at axial location $Z = 3$.

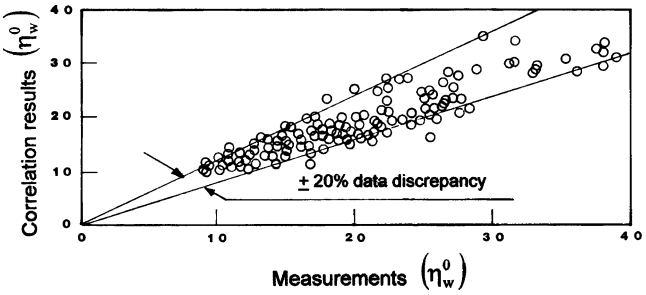

Fig. 9. Comparison of measurements and correlation results of dimensionless wall temperature in static thermosyphon.

correlated by a linear function. A detailed study of the entire data generated with different axial locations shows the similar results typified in Fig. 8 which agreement has led to the proposal that the combined effect of Reynolds number and gravitational Grashof number in the static thermosyphon may be correlated with an equation having the following mathematical structure

$$\eta^0_w = C(Z) + D(Z) \times \frac{Re^2}{Gr_g} \tag{23}$$

where η^0_w is the local dimensionless wall temperature for the static condition and coefficients C and D are functional variables of axial location Z. A detailed examination of the local data gave rise to the proposals shown in Table 4 for the coefficients C and D. Fig. 9 compares the actual measured experimental local dimensionless wall temperatures with those predicted using the empirical correlations given in Table 4. As demonstrated in Fig. 9, 85% of the entire data generated agree with the correlation results with in ±20% difference.

4.2. Reciprocating thermosyphon

When the flow in a heated reciprocating thermosyphon reaches the quasi-steady state, the convective inertia and reciprocating forces couple with buoyancy interaction to generate dynamic periodical flow pattern. This produces the attendant temporal heat transfer variation at each measured

Table 4
Correlations of η_w^0 in static thermosyphon

Z	$\eta_w^0 = C(Z) + D(Z) \times Re^2/Gr_g$	
	$C(Z)$	$D(Z)$
0.5	10.25	8.99E−5
1	11.32	7.29E−5
1.5	12.84	9.98E−5
2	12.8	9.91E−5
2.5	13.6	1.11E−4
3	13.3	1.27E−4
3.5	14.78	1.28E−4
4	14.83	1.30E−4
4.5	14.85	1.32E−4
5	14.87	1.41E−4
5.5	14.95	1.45E−4
6	15.43	1.46E−4

station. After taking the averaged value of the time-wise heat transfer measurements for a period of 10 seconds, the time-averaged heat transfer results are determined. Figs. 10(a)–(c) show the tube-wise distributions of dimensionless wall temperature at Reynolds number of 7100 when the thermosyphon reciprocates at frequencies of 0.83, 1.25 and 1.67 Hz respectively. The axial distributions of dimensionless wall temperature obtained with three ascending heating levels at each *Re*−*Pu* option are compared in each plot of Fig. 10 to show the reciprocating buoyancy effects in isolation. Also the static heat transfer solution evaluated from Eq. (22) is re-produced in Fig. 10 to compare with the results obtained with various reciprocating conditions. The comparative difference between the static and reciprocating results shown in Fig. 10 demonstrates the synergistic effects of inertial force, reciprocating force and buoyancy interaction on heat transfer.

As shown in Fig. 10, the synergistic effects of inertial force, reciprocating force and buoyancy interaction could either increase or reduce the regional dimensionless wall temperatures from the static references of zero-buoyancy. In the hot sealed end of thermosyphon ($Z > 5$), reciprocation could considerably reduce the dimensionless wall temperatures and therefore improves the regional heat transfer. For any *Re*−*Pu* option performed by the present study, the consistent downward data spreads of η_w, driven by the increase of pulsating Grashof number, prevail over the entire thermosyphon. The isolated buoyancy effects in the reciprocating thermosyphon remain persistent to improve heat transfer. The increased dimensionless wall temperatures from the static zero-buoyancy reference in the region of $Z < 5$ as shown in Fig. 10 are thus attributed to the *Pu* effects. The attempt to reveal *Pu* effect on heat transfer with controlled buoyancy level is followed by comparing the heat transfer results obtained with the similar levels of reciprocating Grashof number at a fixed Reynolds number. This is demonstrated in Fig. 11 where the tube-wise distributions of dimensionless wall temperature measured with pulsating numbers of 0.0088, 0.0132, 0.0176 and 0.0212 are compared with the

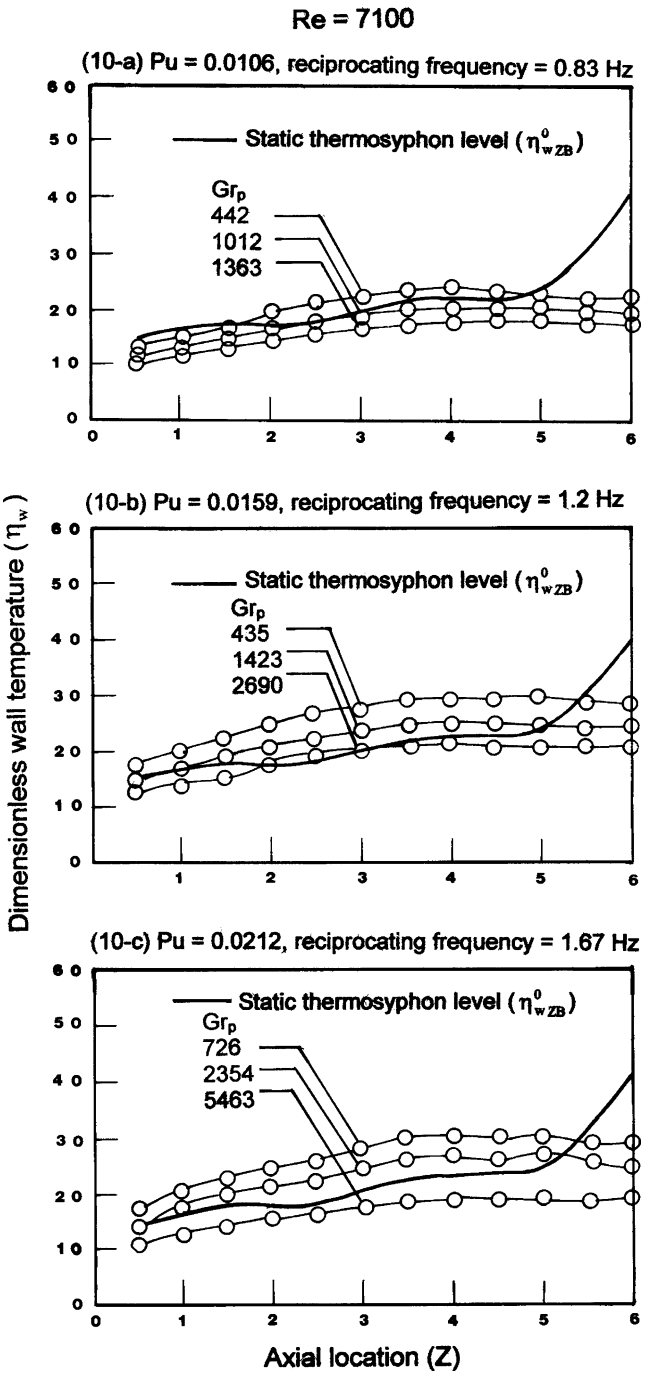

Fig. 10. Axial distributions of dimensionless wall temperature in reciprocating thermosyphon with Reynolds numbers of 7100 at reciprocating frequencies of 0.83, 1.2 and 1.67 Hz.

static zero-buoyancy results for Reynolds number of 8550. Note that Gr_p for this set of reciprocating data is selected at about 1140. The consistent upward data spreads of dimensionless wall temperature driven by increasing pulsating number at fixed values of *Re* and Gr_p are observed in Fig. 11. Heat transfer in reciprocating thermosyphon is gradually reduced when *Pu* increases from 0.0088 to 0.0212. Because Fig. 10 has confirmed that the isolated reciprocating buoyancy effect improves heat transfer, a further increase of

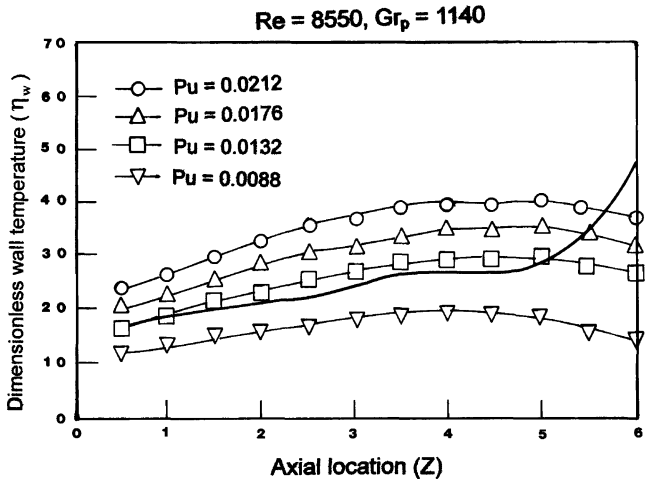

Fig. 11. Axial distributions of dimensionless wall temperature in reciprocating thermosyphon with various pulsating numbers at Reynolds numbers of 8550 and reciprocating Grashof number of 1140.

dimensionless wall temperature from the reciprocating levels depicted in Fig. 11 for the limiting case of zero-buoyancy is clear when the buoyancy levels increase from zero value. In the hot sealed end ($Z > 5$), the values of η_w are initially reduced from the static levels when *Pu* increases from 0 to 0.0088. Following this heat transfer improvement regime is a subsequent impediment when *Pu* is further increased.

The isolation of *Re* variable from Eq. (21) could considerably simplify the strategic task of seeking for the correlating equation that evaluates the individual and interactive effects of inertial, reciprocating and buoyancy forces on heat transfer. To uncouple the effects of *Re* from *Pu* and Gr_p at any axial location in the reciprocating thermosyphon is attempted by normalizing the reciprocating non-dimensional wall temperature with $Re^{n(Z)}$ summarized in Table 3. To demonstrate the isolation of *Re* variable from Eq. (21), two sets of illustrative examples are collected in Fig. 12, where the axial distributions of scaled dimensionless wall temperature in terms of $\eta_w/Re^{n(Z)}$ are produced from three different Reynolds numbers but at the fixed values of pulsating number and reciprocating Grashof number. As seen in Fig. 12(a) and (b), the maximum variation in the scaled dimensionless wall temperature is about 22% of data spread that develops at location of $0.5Z$. The rapid decrease in the *Re* driven data spread appears in the further downstream toward the sealed end of reciprocating thermosyphon. Data generated with three different Reynolds numbers at each pulsating number of 0.0159 or 0.0282 collapses into very tight data band in the axial range of $Z > 1$. The convective force effect in the region of $Z > 1$, quantified by the $Re^{n(Z)}$ relationship in Eq. (22), are demonstrated to be uncoupled from the reciprocating force effects when the η_w is normalized with the equation involving the $Re^{n(Z)}$ structure. As the *Re* variable could be uncoupled from the reciprocating force effects, the individual effect of pulsating force on heat transfer with zero-buoyancy condition is attainable by following the extrapolating procedure illustrated in Fig. 6. As seen in

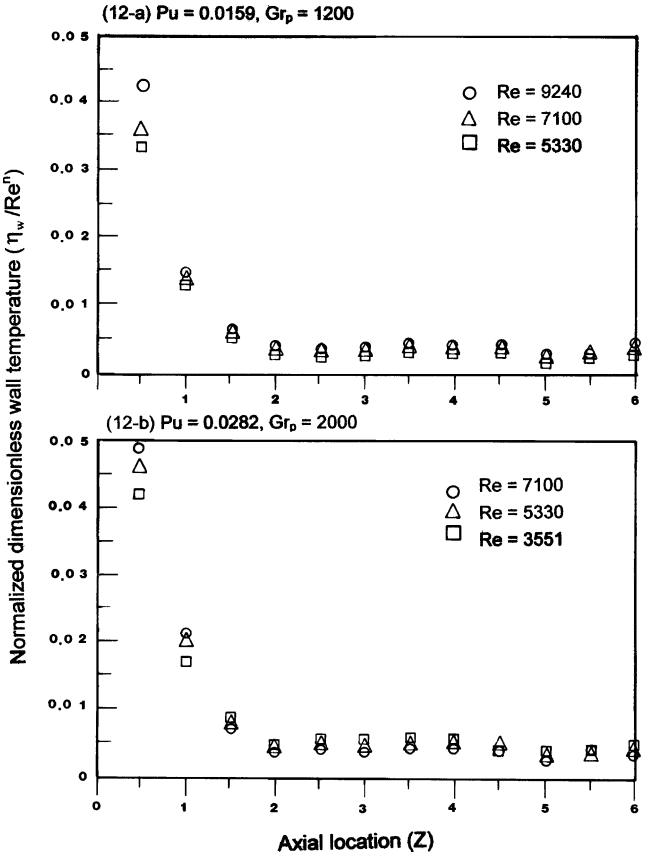

Fig. 12. Axial distributions of normalized dimensionaless wall temperature with different Reynolds numbers at fixed pulsating and reciprocating Grashof numbers.

Fig. 13 where the scaled dimensionless wall temperatures, $\eta_w/Re^{n(Z)}$, generated at fixed pulsating numbers are plotted against reciprocating Grashof number, the data trend decreases linearly when Gr_p increases at each specified pulsating number. The fact that reciprocating buoyancy effect improves heat transfer is reconfirmed. The extrapolation of each data set obtained at the same pulsating number towards the zero Gr_p limit acquires the zero-buoyancy wall temperature data. Therefore the intercept of each linear correlating line depicted in Fig. 13 is treated as the zero-buoyancy heat transfer solution in terms of $\eta_w/Re^{n(Z)}$ which is function of pulsating number and axial location. Note the slope of each correlating line shown in Fig. 13, which varies with pulsating number and axial location, could be treated as an index to assess the degree of buoyancy effect on heat transfer. A large magnitude of the slope represents strong buoyancy effect on heat transfer. The variations of zero-buoyancy heat transfer data with pulsating number from the static zero-buoyancy reference at axial locations of 3, 5.5 and $6Z$ are depicted in Fig. 14. It is typical in the axial region of $Z < 5$ that the normalized dimensionless wall temperatures obtained without buoyancy interaction increase with the increase of pulsating number as demonstrated in Fig. 14. The pulsating force effect alone impairs heat transfer in the axial region of $Z < 5$. However, in the vicinity of sealed end of recipro-

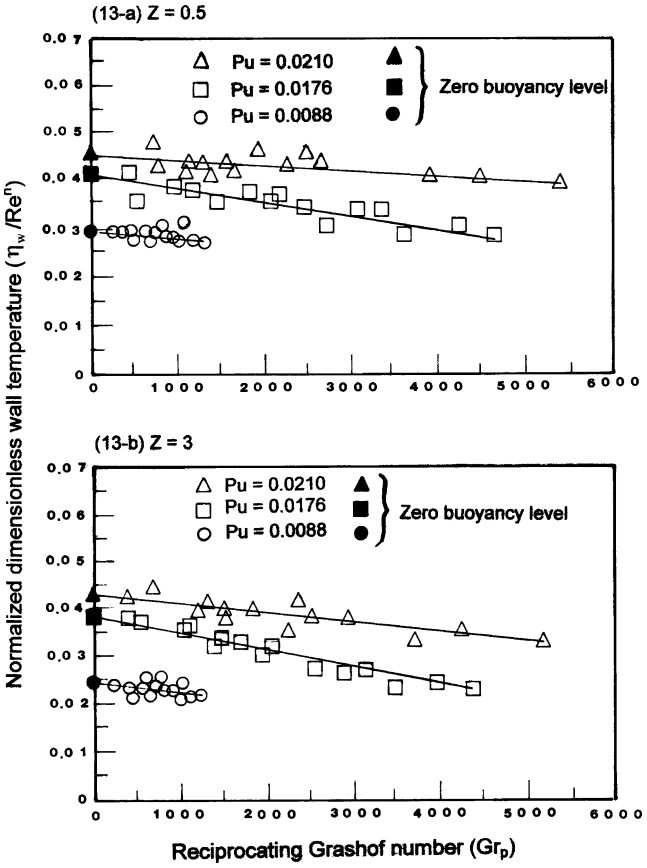

Fig. 13. Variation of dimensionless wall temperature with reciprocating Grashof number in reciprocating thermosyphon for various pulsating numbers of 0.0088, 0.0176 and 0.0212 at axial locations of 0.5Z and 3Z.

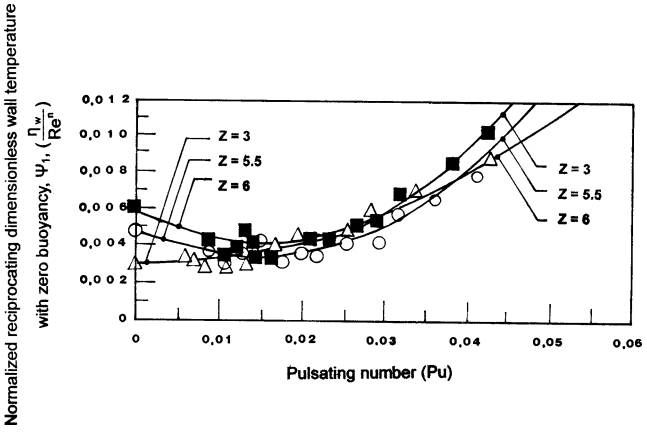

Fig. 14. Variations of zero-buoyancy normalized reciprocating dimensionless wall temperature with pulsating number at axial locations of 3Z, 5.5Z and 6Z.

cating thermosyphon ($Z > 5$), the dimensionless wall temperature affected by the pulsating force alone is initially reduced from the static condition with weak reciprocation, but increases when the pulsating number further increases (see Fig. 14). This heat transfer result at the condition of zero-buoyancy is attributed to the influences of pulsating forces on the vortical flow structures developed in this spatial region. Although the vortical flow structures in the reciprocating thermosyphon appear to be dynamic in nature, the strength of second vortices developed in this spatial region of thermosyphon is initially weakened but subsequently enhanced when the pulsating number gradually increases [14]. Heat transfer affected by pulsating force alone is initially improved at low pulsating number near the sealed end of reciprocating thermosyphon. A subsequent heat transfer reduction in this axial region, that follows the initial heat transfer improvement due to further increase of pulsating number, could lead to considerable heat transfer impediment from the static condition at high pulsating number as demonstrated in Fig. 14. This heat transfer impediment from the static reference caused by the individual pulsating force effect requires particular attention in order to avoid the development of overheating spots in a reciprocating piston.

4.3. Reciprocating heat transfer correlations

The isolated effect of Reynolds number on heat transfer of reciprocating thermosyphon in the axial region of $Z > 1$ is well taken into account via $Re^{n(Z)}$ relationship. Using a series of cross plots, based on Fig. 13, but applied to a range of axial locations, it was possible to interpolate a series of correlating lines for the normalized dimensionless wall temperature against the reciprocating Grashof number for a range of specific buoyancy levels. A linear form of correlating equation, as demonstrated in Fig. 13, is followed by all the axial locations examined so that

$$\frac{\eta_w}{Re^n} = \Psi_1(Pu, Z) + \Psi_2(Pu, Z) \times Gr_p \tag{24}$$

where Ψ_1 and Ψ_2 are functions of pulsating number and axial location. Note that Ψ_1 coefficient features the zero-buoyancy solution that quantifies the individual pulsating force effect. The Ψ_1 value is forced to the A value summarized in Table 3 at zero reciprocating speed ($Pu = 0$) by virtue of the stationary convective solution in the limiting cases of zero-buoyancy. The assumed linear functional form of Eq. (24) with respect to the reciprocating Grashof number permits another simplification in the quest for a correlating equation of heat transfer in reciprocating thermosyphon. As illustrated in previous section, Fig. 14 has depicted the functional shapes of Ψ_1 over a range of axial locations that is treated as zero-buoyancy reciprocating heat transfer data. The manner in which Ψ_2 varies with the pulsating number at the axial locations of 3, 5.5 and 6Z are, respectively, depicted in Fig. 15. The varying pattern typified in Fig. 15 is followed by the results obtained at all the axial locations. Note that the values of Ψ_2 remain negative over the ranges of pulsating numbers and axial locations examined, indicating that the reciprocating buoyancy effect improves heat transfer. As shown in Fig. 15, the influences of reciprocating buoyancy on heat transfer as indexed by Ψ_2 value vary with pulsating number. The existence of coupling pulsating and buoyancy effect on heat transfer in the present reciprocating thermosyphon is therefore demonstrated. There is a minimum

Table 5
Coefficients C_1–C_5

Z	$\Psi_1 = A(Z) + C_1(Z) \times Pu + C_2(Z) \times Pu^2$		$\Psi_2 = C_3(Z) + C_4(Z) \times Pu + C_5(Z) \times Pu^2$		
	C_1	C_2	C_3	C_4	C_5
0.5	−0.4548	31.42	−1.13E−5	7.789E−4	−1.553E−2
1	−0.1428	11.17	−2.38E−6	7.893E−5	−1.65E−3
1.5	−0.1085	5.232	−1.81E−6	7.734E−5	−1.503E−3
2	−0.02975	2.822	−1.18E−6	7.687E−5	−1.484E−3
2.5	−0.03383	2.95	−1.15E−6	7.5E−5	−1.469E−3
3	−0.02911	2.82	−1.25E−6	8.047E−5	−1.543E−3
3.5	−0.0288	2.926	−1.27E−6	8.133E−5	−1.568E−3
4	−0.0289	2.883	−1.23E−6	7.948E−5	−1.553E−3
4.5	−0.053	2.494	−1.22E−6	7.546E−5	−1.536E−3
5	−0.05793	4.09	−1.277E−6	9.667E−5	−1.81E−3
5.5	−0.1672	6.635	−1.349E−6	9.741E−5	−1.779E−3
6	−0.2679	8.846	−1.32E−6	8.805E−5	−1.562E−3

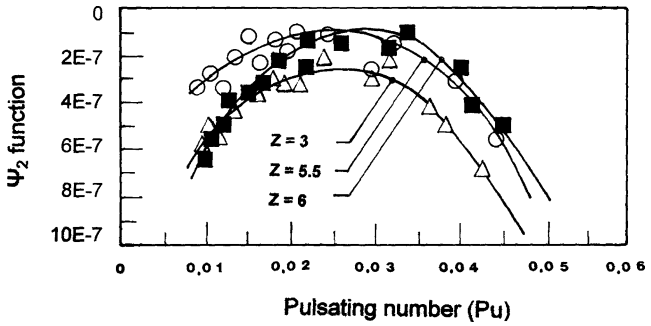

Fig. 15. Variation of Ψ_2 function with pulsating number at axial locations of $3Z$, $5.5Z$ and $6Z$.

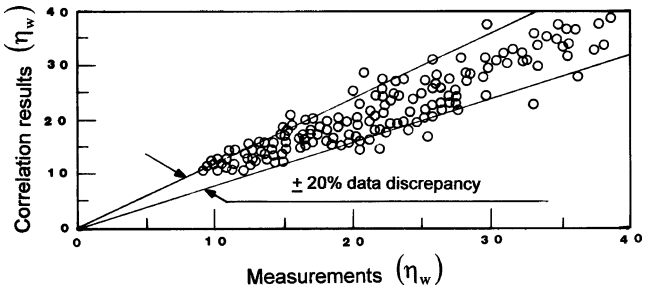

Fig. 16. Comparison of measurements and correlation results of dimensionless wall temperature in reciprocating thermosyphon.

magnitude of Ψ_2 value taking place at the pulsating number in the range about 0.025–0.035 within which the buoyancy effect remains relative weak. Further increase or decrease of the pulsating number from this range results in the increase of the magnitude of Ψ_2 value, which enhances the influence of reciprocating buoyancy on heat transfer. Led by a detailed examination of all axial location versions of Figs. 14 and 15, it is proposed that Ψ_1 and Ψ_2 can be reasonably well correlated by the equations in the following general forms

$$\Psi_1 = A(Z) + C_1(Z) \times Pu + C_2(Z) \times Pu^2 \tag{25}$$

$$\Psi_2 = C_3(Z) + C_4(Z) \times Pu + C_5(Z) \times Pu^2 \tag{26}$$

where C_s are functions of non-dimensional axial location, Z. The numerically determined curve fits for the C_s coefficients are listed Table 5.

The empirical correlation based on a physical interpretation of the governing conservation equations of momentum and energy has been derived following an experimental approach to resolve the influences of inertia force and the coupling effects of pulsating and reciprocating buoyancy forces on heat transfer in a smooth-walled reciprocating anti-gravity open thermosyphon. Comparing all the experimental measurements with the correlative predictions based on Eq. (24) has performed as a review for the overall success of this empirical proposal. Over the entire range of parametric conditions studied, 85% of the present experimental dimensionless wall temperature data are found to agree within ±26% of the correlation proposed. Fig. 16 summarizes the comparison of experimental measurements and correlative results for all the axial locations detected in the reciprocating thermosyphon. Consider the complexities of the flow and heat transfer in the reciprocating anti-gravity open thermosyphon, the proposed correlation could offer a good indication of the individual and combined effects of convective inertial force, pulsating force and reciprocating buoyancy interactions on heat transfer in a smooth-walled reciprocating anti-gravity open thermosyphon.

5. Conclusions

This experimental study examined the heat transfer physics inside a smooth-walled reciprocating square-sectioned anti-gravity open single-phase thermosyphon. The interactive and isolated effects of Re, Gr_g, Pu, and Gr_p on heat transfer along the centerline of heated surface have been particularly studied. In conclusion, the following observations emerge from the data generated within the present parametric ranges tested.

(1) The local dimensionless wall temperature in the static thermosyphon decreases with gravitational Grashof number for all the Reynolds numbers tested, which indicates the improved heat transfer by enhancing buoyancy. Two interacting flow mechanisms, namely the Reynolds number associated flow circulations inside the thermosyphon and the superimposed buoyancy effects, control the heat transfer characteristics of this form of anti-gravity open thermosyphon that could be well correlated in terms of Re^2/Gr_g. A heat transfer correlation, which satisfies both limiting cases of $Pu = 0$ and $Gr_g = 0$, is derived to evaluate the local dimensionless wall temperature along the centerline of the heated surface in the static thermosyphon. In the limiting case of zero buoyancy, the Reynolds number effect on heat transfer is gradually weakened and tend to diminish in the axial region of $Z > 2.5$ when flow approaches the sealed end of static thermosyphon.

(2) The synergistic effects of inertial force, reciprocating force and buoyancy interaction could, respectively, increase or reduce the regional dimensionless wall temperatures in the axial regions of $Z < 5$ and $Z > 5$ from the static reference of zero-buoyancy. The isolated reciprocating buoyancy effect remains persistent to improve local heat transfer. The convective force effects on heat transfer described in terms of $Re^{n(Z)}$ are demonstrated to be decoupled from the influences of reciprocating forces in the axial region of $Z > 1$. This isolated convective force effect increases the dimensionless wall temperature when Re increases. The individual pulsating force effect impairs the heat transfer in the axial region of $Z < 5$. Near the sealed end of the reciprocating thermosyphon, heat transfer affected by pulsating force alone is initially improved at a low pulsating number. A subsequent heat transfer reduction in this axial region is followed after the parametric region of initial heat transfer improvement when the pulsating number continuously increases, which varying tendency could lead to considerable heat transfer impediment from the static condition at high pulsating number. This heat transfer impediment from the static reference caused by the individual pulsating force effect requires particular attention in order to avoid overheating spots in a reciprocating piston.

(3) The proposed correlation of dimensionless wall temperature, which is convenient for engineering applications and consistent with the heat transfer physics, permits the isolated and combined effects of inertial, pulsating and buoyancy forces in the reciprocating smooth-walled anti-gravity open single phase thermosyphon to be taken into account.

Acknowledgement

This work was funded by the National Science Council, Taiwan, ROC toward National Kaohsiung Institute of marine Technology under the grant number, NSC 90-2611-E-022-001.

References

[1] G.H.S. Lock, The tubular thermosyphon, in: Oxford Science Publications, University Press, Oxford, 1992, pp. 286–296.
[2] J.K. Alkire, H. Deligianni, The role of mass transfer on anisotropic electrochemical pattern etching, J. Electrochem. Soc. 135 (1988) 1093–1100.
[3] J.M. Occhialini, J.J.L. Higdon, Convective mass transport from rectangular cavities in viscous flow, J. Electrochem. Soc. 139 (1992) 2845–2855.
[4] L.C. Fang, D. Nicolaou, J.W. Cleaver, Transient removal of a contaminated fluid from a cavity, Internat. J. Heat Fluid Flow 20 (1999) 605–613.
[5] H.S. Kwak, K. Kuwahara, J.M. Hyum, Resonant enhancement of natural convection heat transfer in a square enclosure, Internat. J. Heat Mass Transfer 41 (1998) 2837–2846.
[6] H.S. Kwak, J.M. Hyum, Natural convection in an enclosure having a vertical sidewall with time-varying temperature, J. Fluid Mech. 329 (1996) 65–88.
[7] B.V. Antohe, J.L. Lage, Experimental investigation on pulsating horizontal heating of a water-filled enclosure, ASME J. Heat Transfer 118 (1996) 889–896.
[8] G.Z. Gershuni, D.V. Lyubimov, Thermal Vibrational Convection, Wiley, New York, 1997.
[9] W.S. Fu, W.J. Shieh, A study of thermal convection in an enclosure induced simultaneously by gravity and vibration, Internat. J. Heat Mass Transfer 35 (7) (1992) 1695–1710.
[10] W.S. Fu, W.J. Shieh, Transient thermal convection in an enclosure induced simultaneously by gravity and vibration, Internat. J. Heat Mass Transfer 36 (2) (1993) 437–452.
[11] R.E. Forbes, C.T. Carley, C.J. Bell, Vibration effects on convective heat transfer in enclosures, ASME J. Heat Transfer 92 (1970) 429–438.
[12] S.W. Chang, L.M. Su, C.C. Hwang, T.L. Yang, Heat transfer in a reciprocating duct fitted with transverse ribs, J. Experimental Heat Transfer 12 (1999) 95–115.
[13] Editorial Board of ASME Journal of Heat Transfer, Journal of Heat Transfer Policy on reporting uncertainties in experimental measurements and results, ASME J. Heat Transfer 115 (1993) 5–6.
[14] Y.M. Wang, Experimental study of fluid flow in reciprocating semi-closed cavity, Msc. Thesis, Department of Power Mechanical Engineering, National Tsing Hua University, 2002 (in Chinese).